HTML ABSTRACT + LINKS

Time-resolved electron detachment imaging of the I^- channel in I_2Br^- photodissociation

Richard Mabbs, Kostyantyn Pichugin, Eric Surber, and Andrei Sanov
Department of Chemistry, University of Arizona, Tucson, Arizona 85721-0041

(Received 17 March 2004; accepted 8 April 2004)

The evolution of the I^- channel in I_2Br^- photodissociation is examined using time-resolved negative-ion photoelectron imaging spectroscopy. The 388 nm photodetachment images obtained at variable delays following 388 nm excitation reveal the transformation of the excess electron from that belonging to an excited trihalide anion to that occupying an atomic orbital localized on the I^- fragment. With increasing pump-probe delay, the corresponding photoelectron band narrows on a ~300 fs time scale. This trend is attributed to the localization of the excess-electron wave function on the atomic-anion fragment and the establishment of the fragment's electronic identity. The corresponding band position drifts towards larger electron kinetic energies on a significantly longer, ~1 ps, time scale. The gradual spectral shift is attributed to exit-channel interactions affecting the photodetachment energetics, as well as the photoelectron anisotropy. The time-resolved angular distributions are analyzed and found consistent with the formation of the asymptotic I^- fragment.
© *2004 American Institute of Physics.* [DOI: 10.1063/1.1756869]

I. INTRODUCTION

Chemistry is commonly perceived in terms of atomic rearrangements, yet the motions of atoms result from more fundamental dynamics involving the transformations of the electronic structure. Chemical bonding is controlled by electrons and therefore the underlying goals of time-resolved experiments, or femtochemistry,[1] are best expressed in the context of exploring reactivity and molecular dynamics at the level of electronic structure.

Electrons in molecules are described by their wave functions, i.e., the *eigenfunctions* of the electronic Hamiltonian. However, spectroscopy has traditionally focused on transition frequencies, determined by energy *eigenvalues*. One of the challenges in modern physical chemistry is to shift the experimental focus to probing, in the most direct ways allowed by quantum mechanics, the static and dynamic properties of the electronic wave functions, thus unraveling the driving force of chemistry.

In recent years, the field of negative-ion photoelectron spectroscopy[2] has received a boost from the successful and rapidly expanding application of the imaging technique to the studies of photodetachment of atomic, molecular, and cluster anions.[3–13] Under proper conditions, the two-dimensional snapshots of a photodetached electron cloud yield three-dimensional distributions of the photoelectrons in the laboratory frame, including their speed and angular distributions. The former are easily converted into conventional photoelectron spectra, while the latter reflect the parent orbital symmetry.[7,10,14]

The simultaneous observation of the mutually dependent photoelectron angular distributions and energy spectra is of great benefit to the studies of electronic-structure transformations in several domains important in chemistry, such as the solvent and the reaction-coordinate (or time) domains. In the solvent domain, photoelectron images of size-selected cluster anions reflect the changes in the electronic structure due to electrostatic and covalent intermolecular interactions implicated in cluster and bulk environments.[5,6,8–10] In the reaction-coordinate domain, time-resolved imaging is used to monitor the evolution of the electronic wave function, reflecting the dynamics from the electronic perspective, in real time.[12,13,15–26]

As with many other spectroscopic techniques, time-resolved photoelectron imaging was first introduced in studies of neutral molecules.[24–27] Recently, the Neumark group applied this technique to I_2^- and C_2^- anions,[12,13] combining femtosecond photoelectron spectroscopy (previously developed by the same group)[28–32] with the advantages of negative-ion photoelectron imaging.[3–11,13]

In this paper, we describe a time-resolved photoelectron imaging study of a triatomic anion with multiple dissociation pathways. The photodissociation of I_2Br^- is examined using negative-ion photodetachment as a probe of the dynamics from the electronic perspective. In this report, we monitor the evolution of the I^- fragment channel. The corresponding photoelectron images are recorded in the regime of low electron kinetic energy (eKE). The probe scheme employed emphasizes yet another advantage of imaging: the uniform detection sensitivity over the entire eKE range projected on the detector, especially including the low-eKE region,[6] where traditional (time-of-flight) photoelectron spectroscopy fails. The time-resolved I_2Br^- photoelectron images reflect the evolution of the electronic wave function from the excited molecular anion to the atomic-anion fragment. The results reveal the approximate time scales of excess-electron localization on the fragment and exit-channel interactions.

Trihalide anions play a prominent role in chemistry. Of all the trihalides, I_3^- has received the most experimental and theoretical attention.[32–60] In aqueous solution, the I_3^- absorption spectrum consists of two broad bands centered at 290

 © 2004 American Institute of Physics

and 360 nm.[33] The absorption spectrum is the result of transitions to the mixed $^1\Sigma_{u0}$ and $^3\Pi_{u0}$ states,[34] where the $\Omega=0$ subscripts refer to Hund's case (c) state labeling. Early photolysis studies[35–37] showed that I_2^- is produced from excitation of either band. Time-resolved studies of I_3^- in ethanol indicate a 100% yield of the I_2^- ionic fragments upon excitation of I_3^- at 400 nm[38,39] and 308 nm.[42,43] Excitation towards the blue edge of the higher energy band (266 nm) reveals a decrease in the I_2^- yield due to the opening of another fragmentation channel, presumed to produce I^-+2I.[45] The dynamics of the vibrationally excited I_2^- fragments are characterized by short-time-scale oscillations in transient absorption.[40–44] These oscillations are attributed to coherent semiclassical vibrational motion, followed by the delocalization of the wave packet and relaxation of the nascent nonthermal distribution to a Boltzmann one within 10 ps.[38–43,45–49] In the gas phase, the dissociation dynamics of I_3^- were probed by Neumark's group.[32,58] The experiments at 390 nm indicated a higher degree of nascent I_2^- vibrational excitation compared to the solution phase. In addition, the dissociation channel yielding I^- was observed to be more important, contributing a significant fraction to the dissociation yield over a broad range (420–240 nm).[59]

Compared to I_3^-, very few experimental studies have been carried out on mixed trihalide anions. This is despite the expectation of significantly richer photochemistry due to the increased number of identifiable reaction pathways. The first study of mixed trihalides in the gas phase was carried out by Lineberger and co-workers,[61] who reported the structure and time-resolved photo-dissociation dynamics of $BrICl^-$ and IBr_2^-. The I_2Br^- anion has been previously studied only in solution. In particular, its Raman and infrared spectra have been reported,[62] in addition to a spectrophotometric study of the I_2+Br^- system.[63] More recently, Ruhman and co-workers used I_2Br^- to demonstrate the effects of symmetry breaking on the dynamics of trihalide dissociations.[64,65]

In minimum-energy structures of mixed trihalides the heaviest atom is in the middle.[61,66] For I_2Br^-, two species corresponding to linear I-I-Br$^-$ and I-Br-I$^-$ structures may exist on the ground potential energy surface, but the I-I-Br$^-$ structure is expected to be most stable.[66]

In what follows, we use femtosecond photoelectron imaging of negative ions to monitor the appearance of I^- in the dissociation of gas-phase I_2Br^-. The following section outlines the details of our experimental apparatus pertinent to this time-resolved study. In Sec. III, the emergence of the I^- fragment is monitored by photoelectron imaging, emphasizing the transformation of the excess electron from the molecular to atomic character and its exit-channel interactions with neutral counterfragments.

II. EXPERIMENTAL APPARATUS

The apparatus used in this study employs pulsed negative-ion generation and mass-analysis techniques,[67,68] combined with a velocity-mapped[69] imaging[70] scheme for detection of photoelectrons. The instrument has been described previously in connection with one-photon detachment experiments on atomic, molecular, and cluster anions.[7] Here we present its overview, followed by a more detailed description of the features that enable time-resolved data collection.

The I_2Br^- anions are prepared by crossing a supersonic expansion of IBr seeded in Ar with a beam of high-energy electrons. The precursor mixture is prepared by passing Ar carrier gas at 30 psi gauge through a sample holder containing IBr heated to 30 °C. The resulting mixture is expanded through a pulsed nozzle (General Valve Series 9 with a Kel-F poppet) operated at a repetition rate of 70 Hz into a high-vacuum chamber with a base pressure of 10^{-6} Torr (rising to 3×10^{-5} Torr when the pulsed valve is operated). The supersonic expansion is crossed with a 1 keV electron beam and the resulting anions are pulse extracted into a 2 m long Wiley-McLaren time-of-flight mass spectrometer.[71] After the ion beam is accelerated to about 2.5 keV and focussed using an Einzel lens, it enters the detection region with a typical base pressure of $(3-5)\times10^{-9}$ Torr. The ions are detected mass selectively using a dual microchannel plate (MCP) detector (Burle, Inc.) at the end of the flight tube.

In the pump-probe measurements, I_2Br^- is photolyzed by the 388 nm pump laser beam and the evolving electronic structure is probed via photodetachment with a second, delayed 388 nm laser beam. The pump and probe beams are generated by frequency doubling the output from a regeneratively amplified Ti:sapphire laser system (Spectra Physics Inc.) producing 600 μJ, 100 fs pulses at 777 nm. The fundamental pulse width is monitored using a single-shot autocorrelator (Positive Light SSA). The fundamental radiation is frequency doubled using the 0.1 mm thick BBO crystal of a femtosecond harmonics generator (Super Optronics, Inc.), producing 140 μJ pulses with a bandwidth of 5 nm at 388 nm. The spectral profile of the UV output is monitored using a fiberoptics spectrometer (Ocean Optics, Inc.).

The linearly polarized UV beam is split into the pump and probe using a 50% beam splitter. The separated pump beam passes through a motorized translation stage (Newport ESP300 Universal Motion Controller) to enable controlled temporal separation of the pump and probe pulses. The beams are recombined before entering the reaction chamber using a similar 50% beam splitter. The polarization vectors of the two beams are parallel to each other and to the ion beam axis. Both laser beams are mildly focussed using a 1 m focal length lens positioned approximately 45 cm before the intersection with the ion beam.

The position of zero pump-probe delay is determined by observing a pattern of interference fringes produced when the two coherent beams are overlapped both in time and in space. The variation of the pattern contrast ratio as the delay stage is moved gives an indication of the temporal overlap (cross correlation) of the pump and probe pulses. In the present experiments, the cross-correlation width, as measured before the vacuum chamber entrance window, was determined to be approximately 250 fs. This value defines the approximate time resolution achieved in the experiment.

The 267 nm radiation ($\sim$20 μJ/pulse) used to record the one-photon detachment image of I_2Br^- is obtained by generating the third harmonic of the output of the above laser

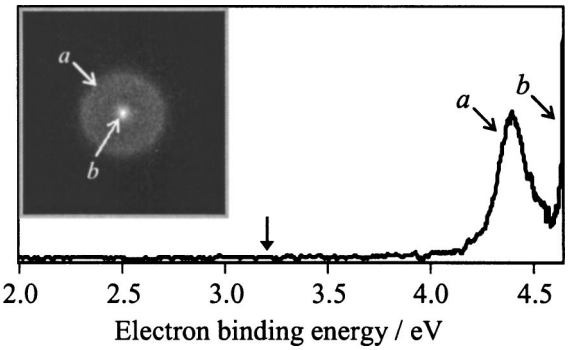

FIG. 1. One-photon photoelectron image and the corresponding spectrum of ground state I_2Br^- recorded at 267 nm. The laser polarization direction is vertical in the image plane. Arrows *a* and *b* indicate the two bands seen in the image (spectrum) at electron binding energies >4 eV. The vertical arrow at 3.2 eV marks the 388 nm pump and probe photon energy used in the time-resolved measurements.

system with the fundamental tuned to 800 nm.

The photodetached electrons are detected using velocity-mapped[69] imaging[70] in the direction perpendicular to the ion and laser beams. A 40 mm diameter MCP detector with a P47 phosphor screen (Burle Inc.) is mounted at the end of an internally μ-metal shielded electron flight tube. Images are obtained from the phosphor screen using a charge-coupled device camera (Roper Scientific Inc.). To suppress background signals, the potential difference across the two MCPs is only pulsed up to 1.8 kV for a 200 ns wide collection window, timed to coincide with the arrival of the photoelectrons. For the rest of each experimental cycle, the dual-MCP potential difference is maintained at 1.0–1.2 kV, which is not enough to produce a detectable signal.

The photoelectron images obtained in a pump-probe experiment contain contributions from the individual pump and probe laser beams, in addition to the true pump-probe signal. These backgrounds are accounted for using a system of mechanical shutters (Uniblitz, Vincent Associates, Inc.) placed in the path of each separated laser beam. The shutters are remotely controlled by the data acquisition system to allow the following pump-probe stages comprising a data acquisition loop: (1) ON-ON, (2) ON-OFF, (3) OFF-ON, (4) OFF-OFF. Each of these stages is typically 10 s (700 experimental cycles) in duration. The pump-probe signal is obtained by subtraction of the ON-OFF (pump only) and OFF-ON (probe only) images from the ON-ON (pump and probe) image. The dark-count background recorded during the OFF-OFF stage is then added to correct for the double subtraction that the above procedure incurs. At each pump-probe delay, the experiment is continuously cycled through stages (1)–(4) until a suitable-quality pump-probe image is obtained. A typical experimental run entails averaging for about 100 of the above four-stage loops, a total of 280 000 experimental cycles. The final images presented in this work were obtained by combining several such runs, representing the result of $\sim 10^6$ experimental cycles.

III. RESULTS AND DISCUSSION

Figure 1 shows a photoelectron image obtained in the one-photon detachment of I_2Br^- at 267 nm. The image represents a projection of the photodetached electron cloud on the plane of the detector. Owing to cylindrical symmetry imposed by the linear laser polarization (vertical in the image plane), the complete velocity (and thus energy), as well as the angular distribution of the photoelectrons can be reconstructed by means of the inverse Abel transformation.[72] The Abel inversion is performed using the BASEX (BAsis Set EXpansion) program of Reisler and co-workers.[73]

The photoelectron spectrum obtained from the 267 nm I_2Br^- image is also shown in Fig. 1. Although the electron affinity corresponding to the formation of I_2Br^- is not known, the photoelectron spectrum consists of two bands with binding energies in excess of 4 eV. Therefore, no one-photon detachment can occur at 388 nm (3.2 eV, indicated by an arrow in Fig. 1) and the absorption at this wavelength can lead only to ionic fragmentation.

One can envisage a range of ionic fragments forming upon excitation of I_2Br^-: Br^-, I^-, I_2^-, and IBr^-. Based on theoretical calculations and analogy with I_3^- and IBr_2^-,[32,57,59,61,66] all four of the above anion fragments should be energetically accessible at 388 nm. Although no gas-phase fragmentation measurements are available for I_2Br^-, past experiments on other trihalides in the gas phase[32,59,61] suggest that both atomic and diatomic anion fragments will indeed be formed by absorption of a pump photon in the present work.

With the 388 nm probe energy, it is feasible to detach electrons from all of the above anion fragments, with the exception of Br^-. In the asymptotic limit (long pump-probe delays), the atomic-anion fragments are expected to yield relatively sharp signatures in the photoelectron images/spectra, while for the diatomic-anion fragments Franck-Condon effects are important. Overall, the photoelectron images may show contributions from one or more reaction channels. In this paper, we focus on the evolution of the I^- channel. Although we do identify a photoelectron band that is tentatively ascribed to the I_2^- and IBr^- channels, these pathways will be the subject of a future publication.

The 388 nm pump–388 nm probe photoelectron images recorded for I_2Br^- at several pump-probe delays are shown Figs. 2(a)–2(e). All images were recorded with the pump and probe laser beams polarized in the vertical direction in the plane of the images. In addition, Fig. 2(f) displays an image corresponding to one-photon detachment of I^- at 388 nm, recorded in a separate experiment on the atomic anion. The images were analyzed using the BASEX program.[73] The resulting photoelectron energy spectra (normalized to unit area) are also shown in Fig. 2.

The delay-dependent changes seen in Figs. 2(a)–2(e) reflect the evolution of the electronic structure of the dissociating trihalide anion. Given our time resolution, the 100 fs image in Fig. 2(a) corresponds to near-zero delay. The image and the corresponding spectrum exhibit two main features: a bright and relatively tight central band (*I*) and a broad anisotropic band peaking around eKE$\approx$1.2 eV (*II*). The latter is seen more clearly in the inset in Fig. 2(a), where the same 100 fs spectrum is shown on a different scale. As the pump-probe delay is increased, the spatial extent of the low-eKE

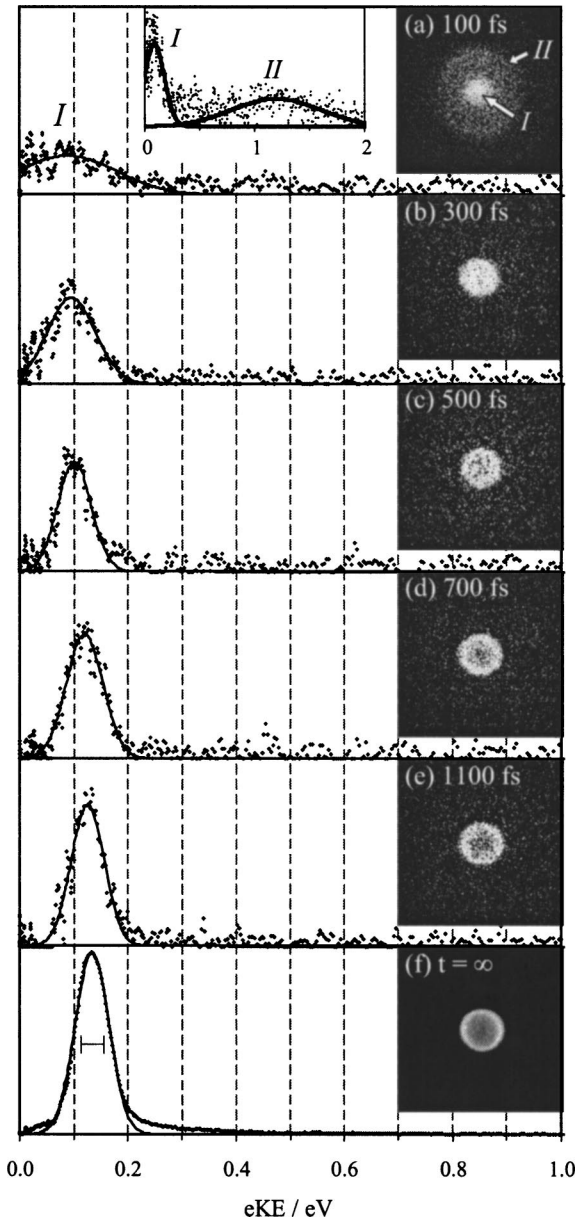

FIG. 2. (a)–(e) 388 nm pump–388 nm probe photoelectron images from I_2Br^- dissociation and the corresponding photoelectron spectra shown in order of increasing delay. All images were recorded with the pump and probe laser radiation polarized in the vertical direction within the plane of the images. The evolving 0.0–0.2 eV peak in the spectra, corresponding to the main feature at the center of all images [marked *I* in (a)], is assigned to the $I_2Br^- \rightarrow I^-$ channel. The inset in (a) shows the 100 fs spectrum on different intensity and energy scales, emphasizing the presence of a second transition (*II*) at higher eKEs. This transition, which is not seen at longer delays, corresponds to the anisotropic outer ring in the 100 fs image. (f) Photoelectron image and corresponding spectrum in one-photon detachment of I^- at 388 nm, effectively representing the I^- channel of I_2Br^- dissociation at infinite pump-probe delay. The solid interval marked in (f) indicates the laser bandwidth (FWHM), not including other experimental broadening factors. Solid lines in (a)–(f) represent Gaussian fits to the peaks seen in the experimental spectra.

feature in the images increases, while the relative intensity at its very center gradually dies away, until a trough can be seen in the center of the image by 700 fs [Fig. 2(d)] and more clearly at 1100 fs [Fig. 2(e)].

To the contrary, the anisotropic higher-eKE band (*II*) appears only at short pump-probe delays, i.e., in the 100 fs image in Fig. 2(a). It can be attributed to two different processes. First, because this signal appears when the pump and probe pulses overlap significantly in time, we cannot rule out a contribution from coherent two-photon absorption by the parent anion. Such absorption is not a true pump-probe process, as both photons can be absorbed from either the pump or the probe beam, in addition to the possibility of simultaneous absorption of one pump and one probe photon. Signals due to the coherent pump-only and probe-only two-photon absorption are not properly accounted for by the background subtraction routine, because their intensity scales nonlinearly with laser power, resulting in the pump-only, probe-only, and pump-probe two-photon signals being nonadditive when the two laser pulses are overlapped in time and space.

The second possible origin of band *II* in Fig. 2(a) is the contribution(s) of the I_2^- and/or IBr^- channel(s). We do not identify any other bands that could be attributed to these channels, even though their yield is expected to be significant at the pump wavelength used. If the higher-eKE band in Fig. 2(a) is indeed due to the diatomic-anion channel(s), its apparent disappearance at longer delays can be due to a combination of dynamic, Franck-Condon, and possibly signal-to-noise factors. The diatomic-anion fragments are formed in highly vibrationally excited states[32,42,43,53,59,61,74] and rapid delocalization of the initially localized time-dependent wave packet[75–80] leads to spreading of the pump-probe signal over a wide energy range. Thus, following the initial rise, the intensity of the pump-probe signals attributed to the diatomic-anion channels drops in time[61] and the resulting diffuse bands[32] are difficult to detect, compared to the sharp transitions associated with atomic-anion channels. The reaction channels yielding diatomic-anion fragments will be addressed in a future publication. In what follows, we focus on the evolution of the 0.0–0.2 eV feature in the images in Fig. 2.

The I^- image obtained in one-photon detachment of the atomic anion at 388 nm is presented in Fig. 2(f) as a reference. It reflects a single photodetachment transition, yielding neutral I atom in the ground $^2P_{3/2}$ state. The upper spin-orbit state $^2P_{1/2}$ lies 0.94 eV higher in energy[81] and is not accessible in 388 nm one-photon detachment. At long delays, the central feature in the time-resolved I_2Br^- images shown in Figs. 2(a)–2(e) clearly converges to a close resemblance of the I^- image, the main difference between Figs. 2(e) and 2(f) being the different signal-to-noise levels. In the spectra, the low-eKE peak in Figs. 2(a)–2(e) shifts to larger eKEs as the delay increases, while the width of the peak decreases, until both the peak position and width become very similar to those of the I^- spectrum in Fig. 2(f). Therefore, the hypothesis emerging from the inspection of the time-resolved photoelectron images in Figs. 2(a)–2(e) is that they reflect the appearance of the I^- fragment in I_2Br^- photodissociation. Hence Fig. 2(f) effectively represents a snapshot of the $I_2Br^- \rightarrow I^-$ channel at infinite pump-probe delay, when the dissociation is complete and the fragments have separated to a distance where they no longer interact.

To parametrize these trends, the bands in the time-resolved spectra are fit with Gaussian functions, as shown in Fig. 2. The corresponding peak positions and widths (ex-

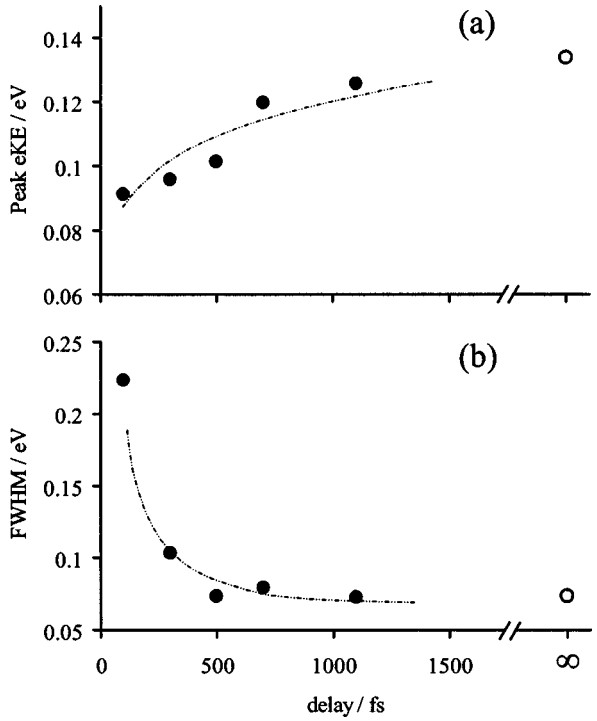

FIG. 3. Evolution of the photoelectron band ascribed to the $I_2Br^- \rightarrow I^-$ channel (388 nm pump–388 nm probe): (a) eKE corresponding to the transition maximum and (b) transition width (defined as FWHM) as functions of pump-probe delay. Filled symbols correspond to time-resolved data from I_2Br^- pump-probe measurements. Open symbols correspond to a one-photon measurement on isolated I^-, representing the $I_2Br^- \rightarrow I^-$ channel in the asymptotic limit of infinite delay. The peak positions and widths are determined by fitting the 0–0.2 eV band in the spectra in Fig. 1 with a Gaussian function. The dashed trend lines, added merely to guide the eye, do not represent quantitative fits to the data.

pressed as full widths at half-maximum, FWHM) are displayed as functions of pump-probe delay in Figs. 3(a) and 3(b), respectively. The peak position evolves gradually with time, on a scale of ~1 ps, approaching an asymptotic maximum value of eKE = 0.13–0.14 eV. The latter corresponds to the detachment energy of I^-, 3.059 eV,[82] subtracted from the 388 nm photon energy, 3.195 eV.

The experimental resolution in the relevant energy range is reflected in the atomic-anion spectrum in Fig. 2(f). The spectral width (FWHM = 0.07 eV) is a convolution of several broadening factors, such as the laser bandwidth [FWHM = 0.04 eV, indicated by a solid interval in Fig. 2(f)] and the ion-beam velocity spread. With all factors considered, it is clear that at long delays the width of the spectral feature approaches the atomic limit.

The widths summarized in Fig. 3(b) approach the asymptotic value of FWHM = 0.07 eV on a time scale of <500 fs. This is of the same order of magnitude as the temporal resolution of the experiment (~250 fs) and therefore the convolution of the reaction kinetics with the pump-probe cross-correlation function must be taken into account. This yields an upper bound of the actual time scale involved in the reaction of about 300 fs.

The width evolution allows two interpretations. First, one can speculate that the excess-electron wave function localizes on the atomic fragment within the first 300 fs and the width of the probe transition reflects the evolving character of the parent orbital, i.e., its transformation from a molecular orbital early in the reaction to a localized atomic orbital at >300 fs. This explanation assumes homogeneous spectral broadening at short delays, due to the molecular nature of the parent orbital. Second, the broader spectrum early in the reaction may also result from inhomogeneous broadening caused by the drift in the peak position with time, within the temporal profile of the pump-probe cross correlation. These two hypotheses are not necessarily exclusive of each other. However, the different time scales of the FWHM and peak-position evolution, revealed by comparing Figs. 3(a) and 3(b), favor the mechanism that relates the width of the photodetachment band to the evolving character of the parent orbital.

The evolution of the photodetached electron energy plotted in Fig. 3(a) indicates that interaction between the departing I^- and its counterfragment(s) persists for ~1 ps, which is significantly longer than the time it takes to establish the atomic-anion character of the I^- fragment. The trend towards larger eKE with increasing pump-probe delay can be attributed to the gradually diminishing solvation of the I^- by the remaining neutral fragments. A different but equivalent view of this process is that the energetic shift is due to the evolving difference between the anion and neutral potentials along the reaction coordinate.

Thus, the atomic-anion character of the I^- fragment appears to be established within <300 fs of excitation, but exit-channel interactions persist for ~1 ps. These time scales must be viewed in the context of molecular-level dynamics. In the case of I_3^-, Neumark and co-workers hypothesized that the I^- fragment is formed via a concerted three-body mechanism.[32,59] However, in more recent work, Zhu *et al.* argued for the additional contribution of two-body dissociation.[60] Although the energetics of I_2Br^- are not so well known,[61,66] the 388 nm pump should be fairly close to the corresponding three-body channel threshold. If we assume, as a crude estimate, a ~0.1 eV kinetic-energy release to I^-, its exit-channel velocity will be ~4 Å/ps. If, on the other hand, the atomic anion is formed via the energetically lower $I^- + IBr$ channel,[32,59,61] greater relative recoil velocities of the final fragments (in the ~10 Å/ps range) can be expected. These are asymptotic estimates; in dissociation on a repulsive potential, the fragment separation starts at a slower, accelerating rate. While the exact details are not known, within a direct dissociation mechanism in the above two energetic regimes the 300 fs time scale corresponds to a displacement of a few Angstroms away from the molecular-anion equilibrium. This is consistent with where the electronic identity of the fragments should have been defined.

The images also reveal the lab-frame photoelectron angular distributions (PADs). In the current pump-probe configuration, the PAD is described by:[83,84]

$$I(\theta) \propto 1 + \beta_2 P_2(\cos\theta) + \beta_4 P_4(\cos\theta), \quad (1)$$

where β_2 and β_4 are anisotropy parameters, P_2 and P_4 are the second- and fourth-order Legendre polynomials, and θ is the angle between the electron velocity vector and the pump and probe polarization direction.

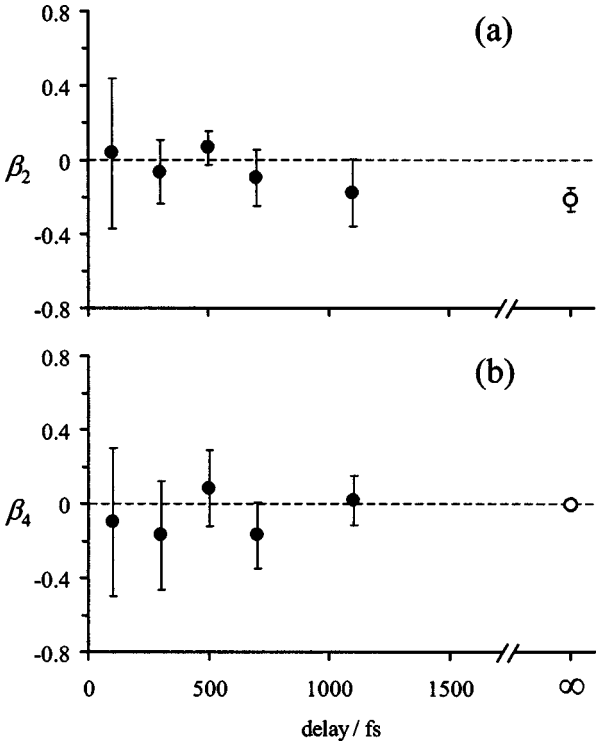

FIG. 4. Evolution of the anisotropy parameters (a) β_2 and (b) β_4 as functions of pump-probe delay in I_2Br^- dissociation via the I^- channel (388 nm pump–388 nm probe). Filled symbols correspond to time-resolved data; open symbols on the right represent one-photon (388 nm) detachment from isolated I^-, representing the $I_2Br^- \rightarrow I^-$ channel in the asymptotic limit of infinite delay. The anisotropy parameters were determined by fitting the 0–0.2 eV band in the photoelectron images shown in Fig. 2 using Eq. (1).

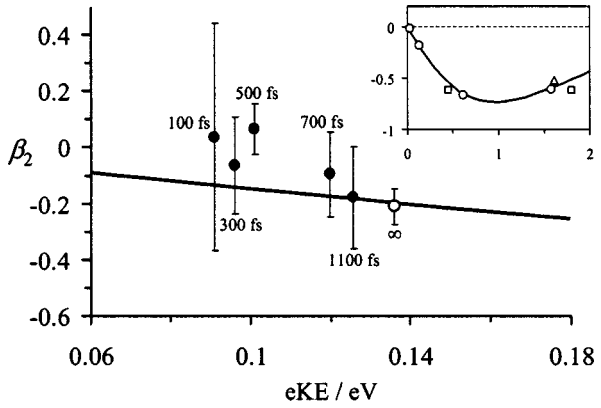

FIG. 5. Comparison of the time-resolved β_2 values obtained in this work to the eKE-dependent values expected for one-photon detachment from I^-. In the main panel, filled symbols represent the time-resolved data at the pump-probe delays indicated next to the data points. The open circle corresponds to one-photon detachment from isolated I^- at 388 nm, representing the limit of infinite pump-probe delay in the I_2Br^- experiment. The solid line represents a fit to the one-photon data using the Hanstorp *et al.* model (Ref. 87), as described in the text. The inset shows the one-photon detachment data for isolated I^- (symbols), for which the model parameters were optimized, and the fitting curve (same as that in the main panel) over a broad eKE range. The open circles represent data obtained in this work and from Ref. 86. The open squares are from Ref. 85 and the open triangle is from Ref. 12.

The PADs corresponding to the I^- channel, determined from the images in Fig. 2, were fit with Eq. (1) using β_2 and β_4 as adjustable parameters. The resulting values of the anisotropy parameters are summarized in Fig. 4, where the values shown represent β_2 and β_4 integrated over the width (at half-maximum) of the spectral profile. Given the modest signal-to-noise ratio in the time-resolved images, special care was taken to assess the reliability of the parameters generated from the data. The PADs were sampled over small radial intervals of varying widths within the spectral profile and the β_2 and β_4 values were determined as means of the individual samples. The error bars in Fig. 4 represent the standard deviation computed through propagation of the uncertainties arising from individual samples. The errors increase significantly at short delays, where the mean eKE of the I^- channel band is small, leading to significant distortions from the center-line noise generated in the Abel inversion.[72]

Within the present limits of uncertainty, no deviations of β_4 from zero could be determined unambiguously. Fundamentally, the β_2 parameter is unaffected by β_4, because of the orthogonality of the P_2 and P_4 Legendre polynomials. Although inspection of the data suggests that β_4 may be important at short delays ($\leqslant$300 fs), ignoring the fourth-order term in Eq. (1), i.e., setting β_4 to zero, at longer delays has insignificant effect on the quality of the fits. This observation is important, because the last term in Eq. (1) arises due to molecular ensemble alignment in a measurement involving the absorption of two photons. The first absorption occurs preferentially in molecules whose transition dipole moments are parallel to the laser polarization axis, thus preparing a partially aligned ensemble of excited intermediates that are probed by the second photon. The departing photofragments, in general, retain a memory of the ensemble alignment, giving rise to nonzero values of β_4.[83,84] However, in the case of the I^- channel, the asymptotic fragment is a closed-shell species. Its electronic wave function is spherically symmetric and therefore incapable of carrying memory of the parent ensemble alignment. Thus, the essentially zero values of β_4 in Fig. 4(b) are not unreasonable, at least at delays $>$300 fs, when the electronic identity of the I^- fragment has already been established.

The variation of β_2 with pump-probe delay, shown in Fig. 4(a), indicates that the PAD is very nearly isotropic up until around 700 fs, after which β_2 increases slightly in absolute magnitude, approaching the bare I^- result ($\beta_2 = -0.18$ at 388 nm). The anisotropy parameter is known to be eKE dependent and hence its variation in time can reflect the changing energy of the detachment transition, as well as the evolving nature of the species probed. To examine the roles of these factors, the β_2 values obtained in the time-resolved $I_2Br^- \rightarrow I^-$ experiment are compared to existing one-photon measurements for I^-. The comparison is shown in Fig. 5, where the solid line represents β_2 as a function of eKE in I^- photodetachment. This curve is obtained by fitting the available one-photon data[12,85,86] to an expression given by Hanstorp *et al.*,[87] which approximates a more rigorous treatment by Cooper and Zare.[14,88,89] The fit over a broad energy range is shown in the inset.[86] The β_2 values from Fig. 4(a) are shown as symbols in the main panel of Fig. 5, where they are plotted against the peak position in the eKE domain.

Overall, good correspondence of the time-resolved data to the asymptotic atomic-anion limit is observed. As eKE

decreases, β_2 for the time-resolved reaction seems to deviate from the isolated I^- case (see Fig. 5, main panel). Although the uncertainties in the present data prevent us from drawing definitive conclusions in this regard, such deviation is to be expected at short delays. Further along the dissociation coordinate, as the excess electron localizes on the atomic fragment and the exit-channel interactions cease (hence, eKE increases), the time-resolved β_2 data points in the main panel of Fig. 5 clearly converge on the curve for isolated I^-. This trend mimics that in Fig. 4(a), where the (same) time-resolved β_2 values approach the I^- limit at long delays. Future experiments probing both the I^- and Br^- channels at shorter probe wavelengths will aim to decrease the uncertainties data and yield further insights into the evolution of photo-electron anisotropy in this reaction.

IV. SUMMARY AND CONCLUSIONS

We have examined the evolution of the I^- channel of I_2Br^- photodissociation using time-resolved negative-ion photoelectron imaging spectroscopy. The 388 nm pump–388 nm probe photoelectron images reveal details of the electronic structure transformation from the excited molecular anion to the atomic-anion fragment. With increasing pump-probe delay, we observe an increase in photoelectron energy corresponding to the asymptotic I^- fragment ($\sim$1 ps time scale), a narrowing of the spectral profile ($\sim$300 fs time scale), and the PAD evolution reflecting the formation of the I^-. Of the above time scales, the shorter one is ascribed to the localization of the excess-electron wave function on the atomic fragment, while the longer time scale reflects the persistence of exit channel interactions, which affect both the energetics of the photodetachment and the resulting PAD.

Thus, the dynamics of the photodissociation can be roughly divided into two stages. During the early stage, the excess-electron wave function transforms from a molecular orbital to a localized atomic orbital. It is during this phase of the reaction that the electronic identity of the fragments is being defined. The second stage involves exit-channel dynamics, during which the products are already defined, but the fragment interactions still persist.

Further experiments on I_2Br^- and other mixed trihalide anions will employ two-color schemes with shorter-wavelength probes to enable the detection of both I^- and Br^- fragment channels, as well as a careful examination of the pathways leading to diatomic-anion fragments.

ACKNOWLEDGMENTS

We gratefully acknowledge discussions with Vladimir Dribinski, one of the developers of BASEX.[73] This work was supported by the National Science Foundation (Grant No. CHE-0134631), the Arnold and Mabel Beckman Foundation (Beckman Young Investigator Award), and the David and Lucile Packard Foundation (Packard Fellowship for Science and Engineering).

[1] A. H. Zewail, J. Phys. Chem. A **104**, 5660 (2000).
[2] K. M. Ervin and W. C. Lineberger, in *Advances in Gas Phase Ion Chemistry*, edited by N. G. Adams and L. M. Babcock (JAI Press, Greenwich, 1992), Vol. 1, p. 121.
[3] B. Baguenard, J. C. Pinare, C. Bordas, and M. Broyer, Phys. Rev. A **63**, 023204 (2001).
[4] B. Baguenard, J. C. Pinare, F. Lepine, C. Bordas, and M. Broyer, Chem. Phys. Lett. **352**, 147 (2002).
[5] E. Surber and A. Sanov, J. Chem. Phys. **116**, 5921 (2002).
[6] R. Mabbs, E. Surber, and A. Sanov, Analyst **128**, 765 (2003).
[7] E. Surber, R. Mabbs, and A. Sanov, J. Phys. Chem. A **107**, 8215 (2003).
[8] E. Surber and A. Sanov, Phys. Rev. Lett. **90**, 093001 (2003).
[9] E. Surber and A. Sanov, J. Chem. Phys. **118**, 9192 (2003).
[10] R. Mabbs, E. Surber, and A. Sanov, Chem. Phys. Lett. **381**, 479 (2003).
[11] H. J. Deyerl, L. S. Alconcel, and R. E. Continetti, J. Phys. Chem. A **105**, 552 (2001).
[12] A. V. Davis, R. Wester, A. E. Bragg, and D. M. Neumark, J. Chem. Phys. **118**, 999 (2003).
[13] A. E. Bragg, R. Wester, A. V. Davis, A. Kammrath, and D. M. Neumark, Chem. Phys. Lett. **376**, 767 (2003).
[14] J. Cooper and R. N. Zare, in *Atomic Collision Processes*, edited by S. Geltman, K. T. Mahanthappa, and W. E. Brittin (Gordon and Breach, New York, 1968), Vol. XI-C, p. 317.
[15] T. Seideman, J. Chem. Phys. **107**, 7859 (1997).
[16] T. Seideman, J. Chem. Phys. **113**, 1677 (2000).
[17] T. Seideman, Phys. Rev. A **64**, 042504 (2001).
[18] T. Seideman, Annu. Rev. Phys. Chem. **53**, 41 (2002).
[19] V. Blanchet, S. Lochbrunner, M. Schmitt, J. P. Shaffer, J. J. Larsen, M. Z. Zgierski, T. Seideman, and A. Stolow, Faraday Discuss. **115**, 33 (2000).
[20] V. Blanchet, M. Z. Zgierski, and A. Stolow, J. Chem. Phys. **114**, 1194 (2001).
[21] M. Schmitt, S. Lochbrunner, J. P. Shaffer, J. J. Larsen, M. Z. Zgierski, and A. Stolow, J. Chem. Phys. **114**, 1206 (2001).
[22] S. Lochbrunner, J. J. Larsen, J. P. Shaffer, M. Schmitt, T. Schultz, J. G. Underwood, and A. Stolow, J. Electron Spectrosc. Relat. Phenom. **112**, 183 (2000).
[23] S. Lochbrunner, T. Schultz, M. Schmitt, J. P. Shaffer, M. Z. Zgierski, and A. Stolow, J. Chem. Phys. **114**, 2519 (2001).
[24] T. Suzuki, L. Wang, and H. Kohguchi, J. Chem. Phys. **111**, 4859 (1999).
[25] L. Wang, H. Kohguchi, and T. Suzuki, Faraday Discuss. **113**, 37 (1999).
[26] J. A. Davies, J. E. LeClaire, R. E. Continetti, and C. C. Hayden, J. Chem. Phys. **111**, 1 (1999).
[27] J. A. Davies, R. E. Continetti, D. W. Chandler, and C. C. Hayden, Phys. Rev. Lett. **84**, 5983 (2000).
[28] M. T. Zanni, T. R. Taylor, B. J. Greenblatt, B. Soep, and D. M. Neumark, J. Chem. Phys. **107**, 7613 (1997).
[29] B. J. Greenblatt, M. T. Zanni, and D. M. Neumark, Chem. Phys. Lett. **258**, 523 (1996).
[30] B. J. Greenblatt, M. T. Zanni, and D. M. Neumark, Science **276**, 1675 (1997).
[31] M. T. Zanni, V. S. Batista, B. J. Greenblatt, W. H. Miller, and D. M. Neumark, J. Chem. Phys. **110**, 3748 (1999).
[32] M. T. Zanni, B. J. Greenblatt, A. V. Davis, and D. M. Neumark, J. Chem. Phys. **111**, 2991 (1999).
[33] A. D. Awtrey and R. E. Connick, J. Am. Chem. Soc. **73**, 1842 (1951).
[34] T. Okada and J. Hata, Mol. Phys. **43**, 1151 (1981).
[35] J. C. Roy, W. H. Hamill, and R. R. Williams, Jr., J. Am. Chem. Soc. **77**, 2953 (1955).
[36] L. I. Grossweiner and M. S. Matheson, J. Phys. Chem. **61**, 1089 (1957).
[37] A. Barkatt and M. Ottolenghi, Mol. Photochem. **6**, 253 (1974).
[38] T. Kühne and P. Vöhringer, J. Chem. Phys. **105**, 10788 (1996).
[39] T. Kühne and P. Vöhringer, J. Phys. Chem. A **102**, 4177 (1998).
[40] T. Kühne and P. Vöhringer, *Ultrafast Phenomena* (Springer, Berlin, 1996), Vol. X, p. 249.
[41] U. Banin, A. Waldman, and S. Ruhman, J. Chem. Phys. **96**, 2416 (1992).
[42] U. Banin and S. Ruhman, J. Chem. Phys. **98**, 4391 (1993).
[43] U. Banin, R. Kosloff, and S. Ruhman, Isr. J. Chem. **33**, 141 (1993).
[44] U. Banin and S. Ruhman, J. Chem. Phys. **99**, 9318 (1993).
[45] T. Kühne, R. Küster, and P. Vöhringer, Chem. Phys. **233**, 161 (1998).
[46] E. Gershgoren, U. Banin, and S. Ruhman, J. Phys. Chem. A **102**, 9 (1998).
[47] U. Banin, R. Kosloff, and S. Ruhman, *Ultrafast Phenomena* (Springer Berlin, 1994), Vol. IX, p. 68.
[48] Z. Wang, T. Wasserman, E. Gershgoren, and S. Ruhman, J. Mol. Liq. **86**, 229 (2000).
[49] S. Hess, H. Bürsing, and P. Vöhringer, J. Chem. Phys. **111**, 5461 (1999).
[50] R. M. Lynden-Bell, R. Kosloff, S. Ruhman, D. Danovich, and J. Vala, J. Chem. Phys. **109**, 9928 (1998).

[51] C. J. Margulis, D. F. Coker, and R. M. Lynden-Bell, J. Chem. Phys. **114**, 367 (2001).
[52] A. E. Johnson and A. B. Myers, J. Chem. Phys. **102**, 3519 (1995).
[53] G. Ashkenazi, U. Banin, A. Bartana, R. Kosloff, and S. Ruhman, Adv. Chem. Phys. **100**, 229 (1997).
[54] E. Gershgoren, S. Ruhman, J. Vala, and R. Kosloff, *Ultrafast Phenomena* (Springer Verlag, Berlin, 2001), Vol. XII, p. 30.
[55] E. Gershgoren, Z. Wang, S. Ruhman, J. Vala, and R. Kosloff, J. Chem. Phys. **118**, 3660 (2003).
[56] E. Gershgoren, J. Vala, R. Kosloff, and S. Ruhman, J. Phys. Chem. A **105**, 5081 (2001).
[57] Y. Ogawa, O. Takahashi, and O. Kikuchi, J. Mol. Struct.: THEOCHEM **424**, 285 (1998).
[58] M. T. Zanni, B. J. Greenblatt, A. V. Davis, and D. M. Neumark, Proc. SPIE **3271**, 196 (1998).
[59] H. Choi, R. T. Bise, A. A. Hoops, and D. M. Neumark, J. Chem. Phys. **113**, 2255 (2000).
[60] L. Zhu, K. Takahashi, M. Saeki, T. Tsukuda, and T. Nagata, Chem. Phys. Lett. **350**, 233 (2001).
[61] A. Sanov, T. Sanford, L. J. Butler, J. Vala, R. Kosloff, and W. C. Lineberger, J. Phys. Chem. A **103**, 10244 (1999).
[62] A. G. Maki and R. Forneris, Spectrochim. Acta, Part A **23**, 867 (1967).
[63] E. Eyal and A. Treinin, J. Am. Chem. Soc. **86**, 4287 (1964).
[64] E. Gershgoren, E. Gordon, D. Star, and S. Ruhman, *Ultrafast Phenomena* (Springer, Berlin, 1996), Vol. X, p. 207.
[65] E. Gershgoren, E. Gordon, and S. Ruhman, J. Chem. Phys. **106**, 4806 (1997).
[66] Y. Ogawa, O. Takahashi, and O. Kikuchi, J. Mol. Struct.: THEOCHEM **429**, 187 (1998).
[67] M. A. Johnson and W. C. Lineberger, in *Techniques for the Study of Ion Molecule Reactions*, edited by J. M. Farrar and W. H. Saunders (Wiley, New York, 1988), p. 591.
[68] M. E. Nadal, P. D. Kleiber, and W. C. Lineberger, J. Chem. Phys. **105**, 504 (1996).
[69] A. T. J. B. Eppink and D. H. Parker, Rev. Sci. Instrum. **68**, 3477 (1997).
[70] D. W. Chandler and P. L. Houston, J. Chem. Phys. **87**, 1445 (1987).
[71] W. C. Wiley and I. H. McLaren, Rev. Sci. Instrum. **26**, 1150 (1955).
[72] A. J. R. Heck and D. W. Chandler, Annu. Rev. Phys. Chem. **46**, 335 (1995).
[73] V. Dribinski, A. Ossadtchi, V. A. Mandelshtam, and H. Reisler, Rev. Sci. Instrum. **73**, 2634 (2002).
[74] U. Banin, R. Kosloff, and S. Ruhman, Chem. Phys. **183**, 289 (1994).
[75] N. Bohr, Z. Phys. **13**, 117 (1923).
[76] E. Schrödinger, Naturwissenschaften **14**, 664 (1926).
[77] L. D. Landau and E. M. Lifshitz, *Quantum Mechanics: Nonrelativistic Theory*, 3rd ed. (Pergamon Press, Oxford, 1977).
[78] I. S. Averbukh and N. F. Perelman, Phys. Lett. A **139**, 449 (1989).
[79] I. S. Averbukh and N. F. Perelman, Sov. Phys. Usp. **34**, 572 (1991).
[80] U. Banin, A. Bartana, S. Ruhman, and R. Kosloff, J. Chem. Phys. **101**, 8461 (1994).
[81] C. E. Moore, *Atomic Energy Level* (U.S. Government Printing Office, Washington DC, 1958), p. 105.
[82] *CRC Handbook of Chemistry and Physics*, 81st ed. (CRC, Boca Raton, FL, 2000).
[83] D. J. Leahy, K. L. Reid, and R. N. Zare, J. Chem. Phys. **95**, 1757 (1991).
[84] K. L. Reid and J. G. Underwood, J. Chem. Phys. **112**, 3643 (2000).
[85] M. K. Gilles, K. M. Ervin, J. Ho, and W. C. Lineberger, J. Phys. Chem. **96**, 1130 (1992).
[86] R. Mabbs, E. S. Surber, and A. Sanov (unpublished).
[87] D. Hanstorp, C. Bengtsson, and D. J. Larson, Phys. Rev. A **40**, 670 (1989).
[88] J. Cooper and R. N. Zare, J. Chem. Phys. **48**, 942 (1968).
[89] J. Cooper and R. N. Zare, J. Chem. Phys. **49**, 4252 (1968).